PROTEINS: Structure, Function, and Genetics 34:96–112 (1999)

Tertiary and Quaternary Conformational Changes in Aspartate Transcarbamylase: A Normal Mode Study

Aline Thomas,[1] Konrad Hinsen,[1] Martin J. Field,[1]* and David Perahia[2]
[1]*Laboratoire de Dynamique Moléculaire, Institut de Biologie Structurale—Jean-Pierre Ebel, Grenoble, France*
[2]*Laboratoire de Modélisation et d'Ingénierie des Protéines, Université d'Orsay, Orsay, France*

ABSTRACT **Aspartate transcarbamylase (ATCase) initiates the pyrimidine biosynthetic pathway in *Escherichia coli*. Binding of aspartate to this allosteric enzyme induces a cooperative transition between the tensed (T) and relaxed (R) states of the enzyme which involves large quaternary and tertiary rearrangements. The mechanisms of the transmission of the regulatory signal to the active site (60 Å away) and that of the cooperative transition are not known in detail, although a large number of single, double, and triple site-specific mutants and chimeric forms of ATCase have been obtained and kinetically characterized. A previous analysis of the very low-frequency normal modes of both the T and R state structures of ATCase identified some of the large-amplitude motions mediating the intertrimer elongation and rotation that occur during the cooperative transition (Thomas et al., J. Mol. Biol. 257: 1070–1087, 1996; Thomas et al., J. Mol. Biol. 261:490–506, 1996). As a complement to that study, the deformation of the quaternary and tertiary structure of ATCase by normal modes below 5 cm^{-1} is investigated in this article. The ability of the modes to reproduce the domain motions occurring during the transition is analyzed, with special attention to the interdomain closure in the catalytic chain, which has been shown to be critical for homotropic cooperativity. The calculations show a coupling between the quaternary motions and more localized motions involving specific residues. The particular dynamic behavior of these residues is examined in the light of biochemical results to obtain insights into their role in the transmission of the allosteric signal. Proteins 1999;34:96–112.** © 1999 Wiley-Liss, Inc.

Key words: aspartate transcarbamylase; allostery; quaternary and tertiary motions; normal mode analysis; low-frequency modes

INTRODUCTION

Aspartate transcarbamylase (ATCase) catalyzes the synthesis of N-carbamyl-L-aspartate from L-as-partate and carbamyl phosphate; it is the first enzyme in the pyrimidine synthesis pathway.[3–5] The reaction is cooperative and regulated by allosteric effectors. It is feedback inhibited by cytosine 5′-triphosphate (CTP) and activated by adenosine 5′-triphosphate (ATP). Several crystal structures of ATCase from *Escherichia coli* bound to different effectors and substrate analogs have been determined.[3,4] ATCase is a dodecamer containing six catalytic (C) chains of 310 residues each and six regulatory (R) chains of 153 residues each. It is structurally organized into two C chain trimers and three R chain dimers (see Fig. 1). The complex has full C_3 symmetry. The deviation from D_3 symmetry is due to the existence and distribution of CTP-binding sites of two different affinities.[3,5–7]

Each catalytic chain is divided into two domains, the carbamyl phosphate domain (CP domain) and the aspartate domain (ASP domain). Each contains a β-sheet surrounded by α-helices and is interconnected by the α-helices H5 and H12 (see Table I). The active site is shared between two adjacent catalytic chains. The regulatory chains are also composed of two domains each of which has a β-sheet and a binding site. The allosteric domain (ALLO domain) contains the effector that binds at the R1:R6 interface, and the zinc domain (ZN domain) contains a structural zinc atom located at the R1:C1 interface.

Binding of aspartate to the active site induces the cooperative transition of ATCase from the low affinity tensed (T) state to the high activity, high affinity relaxed (R) state. The T → R transition involves large quaternary rearrangements such as an 11 Å increase in the intertrimer distance, a 12° rotation of the trimers relative to one another, and a 15° rotation of the regulatory dimers around their pseudo 2-fold axes. Large modifications of the tertiary structure accompany the aspartate binding. There is an opening[4] of the cleft between the ALLO and ZN domains by a rigid-body rotation of about 9°. The ASP domain also moves as a rigid body toward the CP domain by about 3 Å, resulting in closure of the active site.[8] The 80s and 240s loops are displaced by about 5 and 10 Å, respectively.[4]

ATCase is a highly flexible protein and the binding of all ligands to ATCase induces structural modifications. Binding of carbamoyl-phosphate to the wild-type enzyme has been shown by ultraviolet (UV) and difference circular dichroism to provoke large three-dimensional perturba-

Grant sponsor: Institut de Biologie Structurale—Jean-Pierre Ebel (CNRS/CEA); Grant sponsor: Human Frontiers Science Program.
*Correspondence to: Martin J. Field, Laboratoire de Dynamique Moléculaire, Institut de Biologie Structurale—Jean-Pierre Ebel, 41 Avenue des Martyrs, 38027 Grenoble Cedex 1, France.
Received 24 April 1998; Accepted 11 August 1998

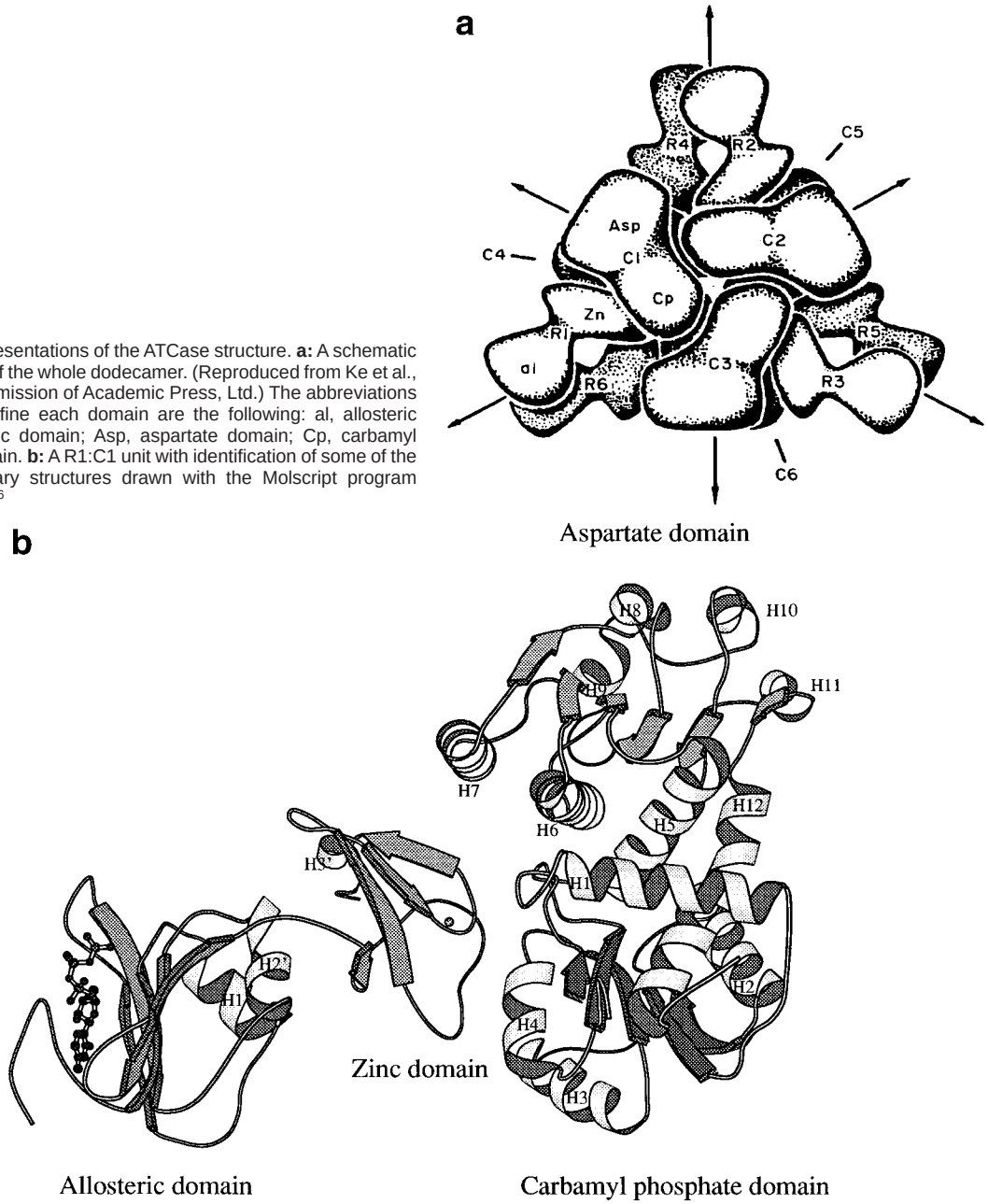

Fig. 1. Representations of the ATCase structure. **a:** A schematic representation of the whole dodecamer. (Reproduced from Ke et al., 1988,[55] with permission of Academic Press, Ltd.) The abbreviations employed to define each domain are the following: al, allosteric domain; Zn, zinc domain; Asp, aspartate domain; Cp, carbamyl phosphate domain. **b:** A R1:C1 unit with identification of some of the regular secondary structures drawn with the Molscript program (Kraulis, 1991).[56]

tions of the enzyme.[9,10] Nucleotide binding also modifies the internal arrangement of the enzyme: both CTP and ATP cause a small increase and decrease in the average separation between the catalytic trimers, respectively.[7,11] Intermediate states between the T and R state crystal forms have been obtained by site-directed mutagenesis studies.[12,13] Mutated ATCase can adopt a restrained T state structure[14] or R state[15] despite the presence or absence of the substrate or effector. Moreover, diffuse X-ray scattering has demonstrated that in solution, the R state enzyme does not adopt the same structure as in the crystal environment.[16]

The high flexibility of ATCase makes it a very attractive candidate for theoretical studies focused on large amplitude motions. Previous theoretical studies have included a molecular dynamics (MD) simulation[17] and normal mode (NM) analyses.[1,2] The advantage of the NM method is that it allows the decomposition of the full molecular motion into discrete vibrational motions that can be studied separately, so that the large amplitude motions corresponding to low-frequency modes can be selectively analyzed.[18] To access these delocalized motions by the MD technique, very long simulations are required and special filtering techniques need to be applied to remove contributions

TABLE I. Definition of the Different Substructures in ATCase as Referred to in the Text†

	Secondary structure	Residue numbers
Catalytic chain		
CP domain	S1	7–9
	T1	11–14
	H1	17–32
	S2	42–48
	H2	53–66
	S3	68–74
	H3	88–98
	S4	101–106
	H4	111–119
	S5	123–127
	T2	129–132
	Sheet_1	S1, S2, S3, S4, S5
Inter-CP-ASP domain	H5	135–149
	H12	285–305
ASP domain	S6	155–160
	H6	167–179
	S7	182–188
	T3	189–192
	H7	196–205
	S8	208–212
	H8	215–220
	S9	224–230
	H9	237–242
	H10	251–256
	S10	262–265
	H11	275–279
	S11	281–283
	Sheet_2	S6, S7, S8, S9, S10, S11
Loops	80s loop	76–85
	240s loop	225–245 (S9-H9)
Regulatory chain		
Allosteric domain	S1′	14–19
	H1′	25–33
	S2′	41–46
	S3′	55–62
	H2′	69–77
	S4′	82–87
	S5′	93–97
	Sheet_3	S1′, S2′, S3′, S4′, S5′
Zinc domain	S6′	102–104
	S7′	123–129
	S8′	135–138
	S9′	143–146
	H3′	147–150
	Sheet_4	S6′, S7′, S8′, S9′
First trimer	Catalytic chains C1, C2, C3, symmetrically equivalent through C_3 operation	
Second trimer	Catalytic chains C4, C5, C6, symmetrically equivalent through C_3 operation	

†S: β-strand; H: α-helix; CP: carbamyl phosphate; ASP: aspartate. (Partially from Lipscomb[3]; Reproduced from Ke et al., 1988[55] with permission of Academic Press, Ltd.)

from the more localized higher frequency atomic motions, i.e., "background" fluctuations.[19] In the case of hemoglobin, the second lowest frequency mode corresponds to the transition from the T to R state,[20] and is similar to the path obtained by MD simulations of this protein (Lechheb et al., personal communication). NM simulations reproduce experimental data such as crystallographic B factors and diffuse X-ray scattering patterns,[21] and it has been shown recently that the directions of the motions of the very low-frequency normal modes are strongly conserved among different protein configurations.[22]

In our previous NM[1,2] calculations of the CTP-ligated T and CTP-ligated R crystal forms of ATCase, we identified motions in the protein with periods ranging from 70 ps to 7

ps (equivalent to frequencies of between 0.5 and 5 cm^{-1}). Our analyses showed that the contribution to the overall cooperative transition of the motions arising from these low-frequency modes was significant. Indeed, some of the mode motions generated a gear-wheel motion that is very close to the mechanism of the quaternary transition deduced from the crystal structures.[23] We believe that these observations, in conjunction with the other evidence discussed above, lend support to the use of NM analyses of single structures to identify motions that could be implicated in large scale conformational transitions in proteins.

In this article, we extend the analyses of our previous two papers[1,2] and investigate the quaternary and tertiary structural modifications resulting from the very low-frequency motions in both the CTP-ligated T and R state ATCase structures. The quaternary structural changes we are concerned with are the relative motions between the ASP and CP domains and between the ALLO and ZN domains.

MATERIALS AND METHODS

Modeling the Structures

The procedure used for modeling the initial structures for the NM calculations has been described in detail elsewhere[1,2] and so only a brief description will be given here. The initial crystal structures were the following: the T state structure[24] refined to 2.5 Å and liganded with CTP and zinc and the R state structure[7] refined to 2.8 Å and liganded with CTP, zinc, malonate, and phosphonoacetamide. Polar hydrogens were added to these crystal structures with the HBUILD algorithm.[25] The protonation states of the residues were chosen so as to mimic an environment at pH 7. The histidines were neutral and their enantiomers were taken as those previously assigned when possible[24] or so as to optimize favorable interactions otherwise. The CTP parameters had to be modeled from a combination of ATP and cytosine parameters. For the malonate parameters, we used those of glutamic acid and the phosphonoacetamide parameters were derived from those of N-(phosphonoacetyl)-L aspartate[26] and CTP. The sets of coordinates were smoothly minimized with the ABNR algorithm[27] with a protocol preventing a strong deviation from the initial structure and from the C_3 symmetry of the dodecamers.

Essential conditions for the minimization were a linear distance-dependent dielectric constant,[28] a shifted electrostatic potential, and a switched van der Waals potential.[29] The cutoff for nonbonded interactions was set to 11 Å. The water screening effect was modeled by weighting the atomic charges of the ends of the charged amino acid side chains (Lys, Arg, Glu, Asp) by 0.3.[30] The charges on all ligands were modified similarly. The T state structure contained 26,586 atoms in total, while the R state structure contained 26,472 atoms.

NM Calculations

All calculations were performed with the CHARMM-22 molecular modeling software,[27] using the empirical force field parameters from the QUANTA-21 program (Molecular Simulations, Inc., San Diego, CA). The DIMB method (diagonalization in a mixed basis set)[31,32] was used to perform the NM calculations. This recent method is particularly well suited for the determination of the low-frequency normal modes in large molecular systems.[30,33] It uses an iterative procedure that converges from a set of initial trial modes to the refined lowest frequency ones within a given error tolerance. Due to computer memory limits, we obtained only the 53 lowest frequency normal modes for both the T and R structures. The corresponding frequencies ranged from 0.58 to 3.81 cm^{-1} for the R structure and from 0.54 to 4.09 cm^{-1} for the T structure. Due to the C_3 symmetry of the system, the vibrational modes can be characterized as nondegenerate modes showing symmetric motions about the C_3 axis and pairs of degenerate modes that have the same frequency and that produce displacements that break the symmetry.[34]

Structure-Based Analysis

The influence of the NM motions on three geometrical features was studied: the interresidue distances, the interdomain rotation angles, and the backbone dihedral angles. The variation in these quantities in the minimized reference structure called S_0, and in two structures called S_{+1}, S_{-1}, obtained by displacing S_0 along the NM eigenvector with an amplitude corresponding to a temperature of 600 K in both directions (300 K in the case of interdomain rotation angle), is a characteristic of the NM effect on the structural deformation.

The interresidue distance variation is defined as

$$D^k_{i,j} = |d^k_{i,j}(S_{+1}) - d_{i,j}(S_0)| + |d^k_{i,j}(S_{-1}) - d_{i,j}(S_0)|$$

where $d^k_{i,j}(S_A)$ is the distance between the Cα atoms of residues i and j in structure S_A, ($A = -1$ or $+1$) displaced along mode k. $d_{i,j}(S_0)$ is the corresponding distance in the minimized structure. The sum over all 53 normal modes of the distances $D^k_{i,j}$, as expressed in $D_{i,j} = \Sigma^{k=53}_{k=1} D^k_{i,j}$ describes the total modification of this distance for vibrations between 0.5 and about 4 cm^{-1}, and is represented in Figure 2a,c. The difference distance map between the crystal T and R structures corresponding to the distribution of the following quantity: $D^{X\text{-}RAY}_{i,j} = |d_{i,j}(T) - d_{i,j}(R)|$ is represented in Figure 2b,d.

The backbone flexibility around each residue i was characterized by the parameter θ^k_i, which is a measure of the backbone dihedral angle variation when the structure is displaced along mode k:

$$\theta^k_i = |\theta^k_i(S_{+1}) - \theta^k_i(S_{-1})|$$

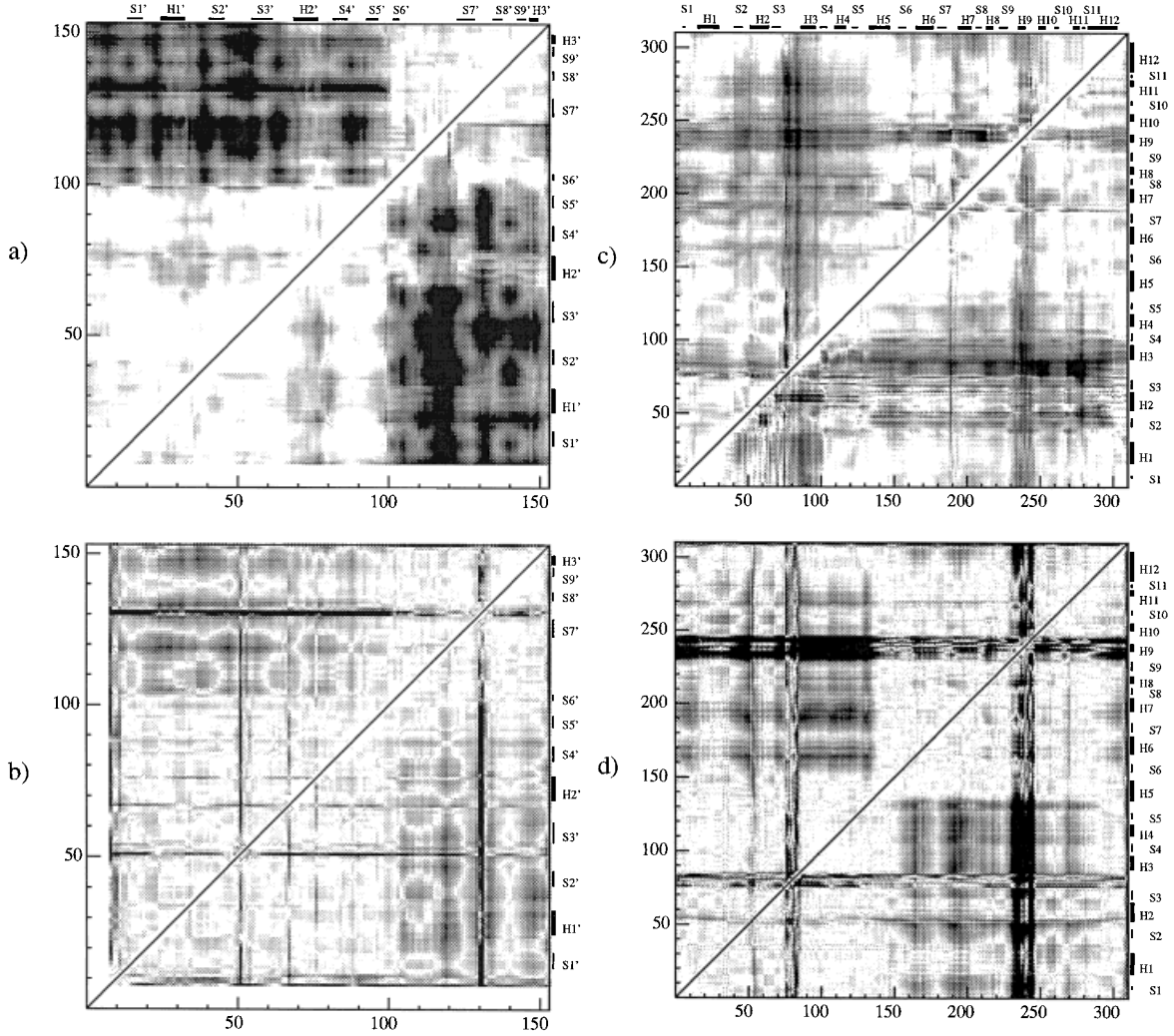

Fig. 2. Interresidue distance variation maps. **a:** In chain R1 as a result of the low-frequency modes: in the T state (upper diagonal) and in the R state (lower diagonal) structures. **b:** In chain R1 from the difference between the crystal T and R structures (both diagonal parts). **c:** In chain C1 as a result of the low-frequency modes: in the T state (upper diagonal) and in the R state (lower diagonal) structures. **d:** In chain C1 from the difference between the crystal T and R structures (both diagonal parts). The darker the dots, the larger the distance variations. The absence of dots means that the corresponding distance variation is negligible.

The ω angles do not show significant variations, while the ϕ and ψ angles often show simultaneous and similar variations within the same residue (data not shown). Consequently, we present the total of the mean variations of the ϕ and ψ backbone angles among all of the 47 normal modes in Figure 3. For comparison, the averaged difference in the ϕ and ψ angles between the T and R crystal structures is also presented in Figure 3.

For structures displaced along the modes, we present in Figure 4 the following quantity:

$$\Delta_k^{chain} = |a_k(S_{+1}) - a^0| + |a_k(S_{-1}) - a^0|$$

which quantifies the deformation by mode k of the interdomain rotation angle and represents the relative change in interdomain rotation angle when the system is displaced along mode k compared to the interdomain rotation angle between the minimized T and R structures. $a_k(S_{+1})$ is the difference in interdomain rotation angle when the system goes from configuration S_0 to configuration S_{+1} and is calculated as follows: the Cα atoms of domain i within chain A in configuration S_0 are fitted[35,36] on the corresponding atoms in configuration S_{+1}, and then the Cα atoms of domain j within chain A in configuration S_0 are fitted on the corresponding atoms in configuration S_{+1}. The angle a^0 is the same angle calculated using the minimized T and R configurations. Table II lists the interdomain rotation angle differences between the minimized structures and also for the crystal structures. The angle between the ASP and CP domains is given when *chain* is C1 or C6, while the

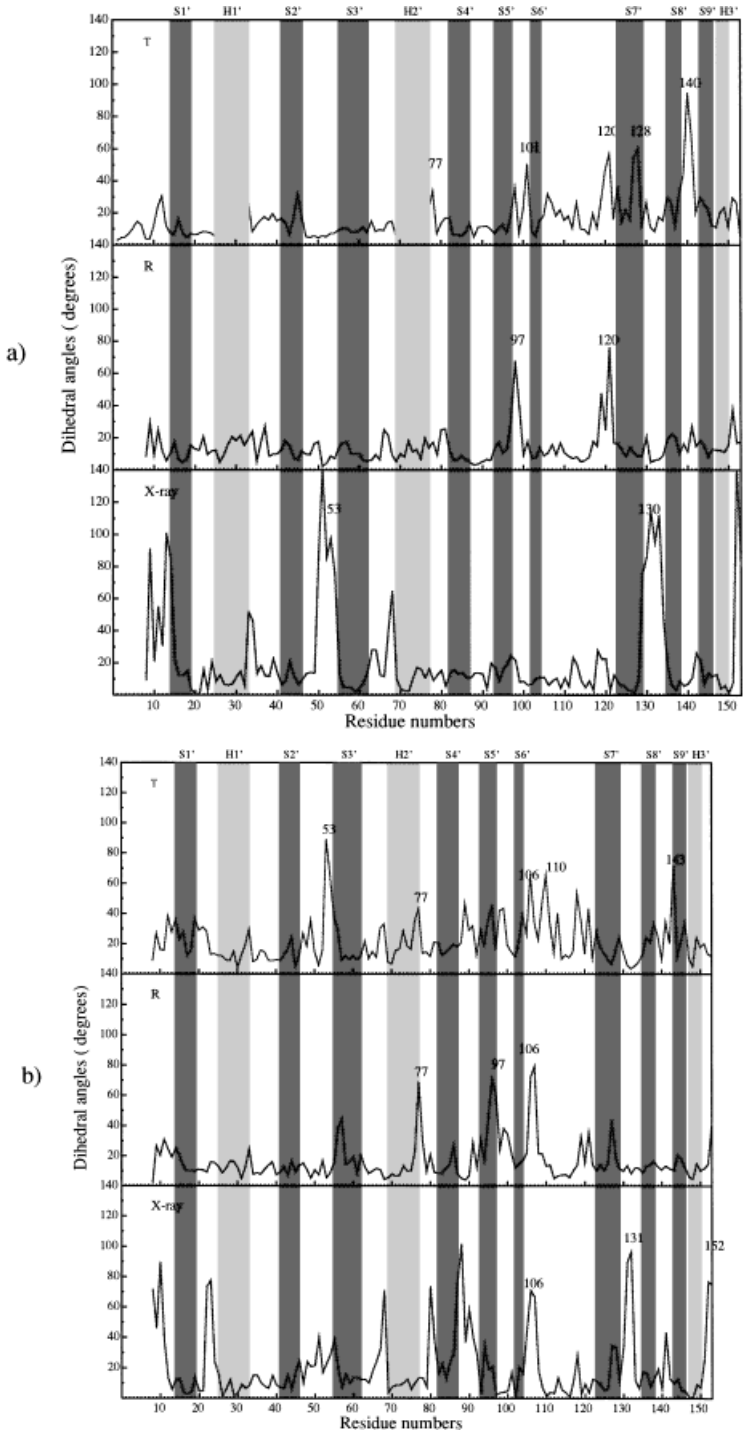

Fig. 3. The backbone dihedral angle variations due to the calculated normal modes in the T (**top**) and R (**middle**) states and to the overall transition deduced from a comparison of the crystal T and R state structures (**bottom**). **a:** In the R1 chain. **b:** In the R6 chain. **c:** In the C1 chain. **d:** In the C6 chain.

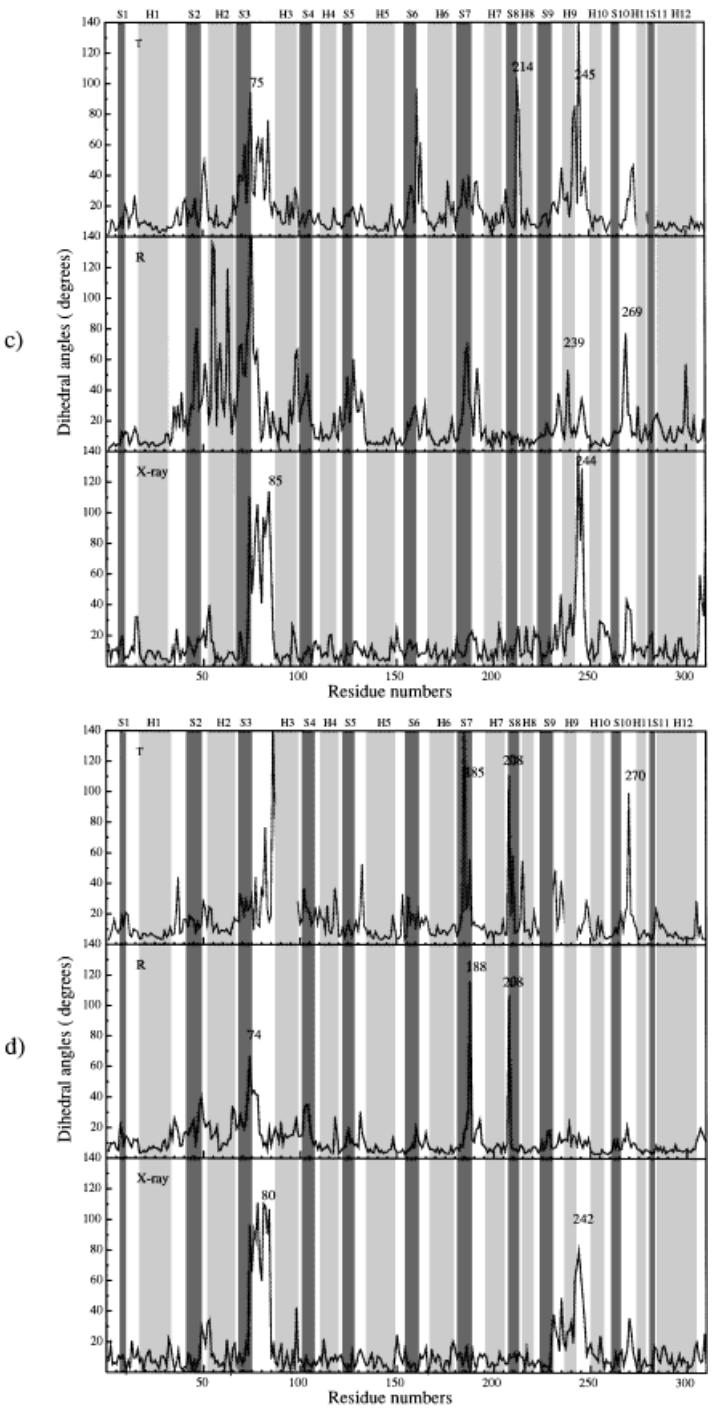

Figure 3. (Continued.)

angle between the ALLO and ZN domains is given when *chain* is R1 or R6.

The coordinates of the first seven residues of the regulatory chains in the R state were missing in the crystallographic structure due to crystal disorder, and thus they are also omitted from the related analyses.

Vector-Field Analysis of the NM Motions

A technique based on vector analysis and implemented in the molecular modeling toolkit[37] was used to investigate the structural deformations due to the normal modes. The atomic displacements associated with a normal mode or

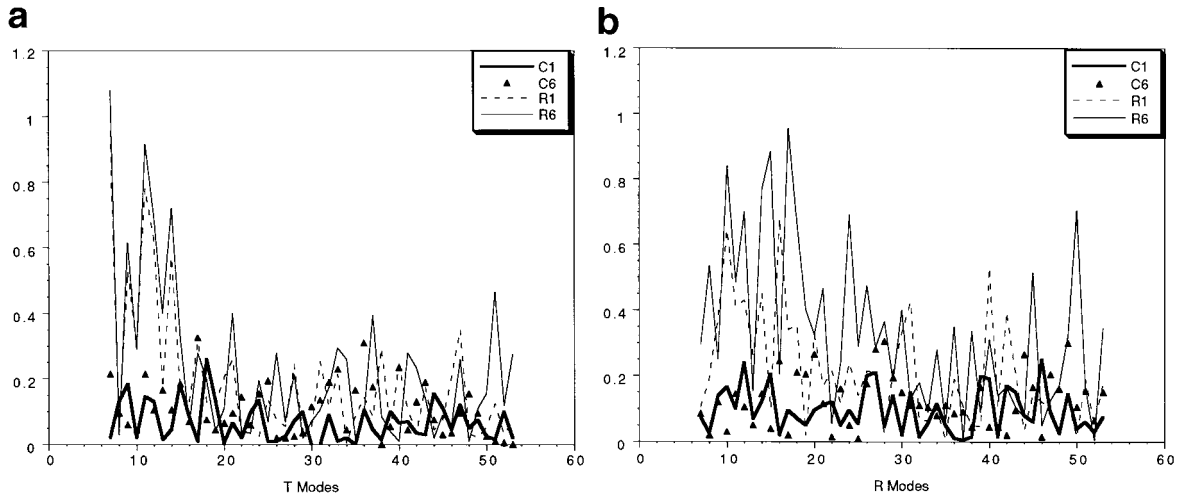

Fig. 4. The interdomain rotation angle deformation parameter, Δ_k^{chain}, as a function of the mode number for (**a**) the T state modes and (**b**) the R state modes.

TABLE II. Differences in the Interdomain Angles of Rotation (in Degrees)[†]

Chain	A	B
R1	12.30	20.79
R6	15.94	25.21
C1	12.63	15.65
C6	13.16	11.99

[†]A: Between crystal structures; B: between minimized structures. The domains are defined in residue numbering as follows: ALLO[14;97], ZN[102:150], CP[7:132], ASP[155:283].

with the T → R transition can be interpreted as the values of a vector field, defined everywhere in space at the positions of the atoms, which can be studied using established techniques of vector analysis. For the low-frequency modes the vector field will vary slowly in space, which permits its calculation by spatial averaging over small regions. These regions were chosen to be cubes with an edge length of 5 Å, containing on average 6 atoms each. The vector field $\vec{u}$, defined on a regular lattice at the center of each cube, is the mass-weighted average of the displacements of the atoms in the cube, and is called the displacement field (see Fig. 5).

Since the integral over the vector field is zero (the normal modes are orthogonal to the three zero-frequency translation modes), it is fully characterized by its nine derivatives, which form a tensor of rank 2 at each point in space, written as $\vec{\nabla}\vec{u}$. This tensor can be decomposed into three irreducible tensors of ranks 0, 1, and 2: the divergence, $\vec{\nabla} \cdot \vec{u}$, which describes the local change of density; the curl, $\vec{\nabla} \times \vec{u}$, which describes the local rotation field; and the symmetric and traceless part, $\overline{\vec{\nabla}\vec{u}}$ which describes the local deformation (strain) due to the vector field.

Regions of rigid-body motion are characterized by a constant curl which gives the axis and the magnitude of the rotation. The deformation and density changes describe local rearrangements of atoms; since such changes involve large energies and hence high-frequency motion, they are small for the low-frequency modes studied here, except in regions of very large flexibility. The total divergence, calculated as the sum of the divergence over all modes and averaged over all atoms of a residue, allows a quantitative analysis of the local flexibility, and is presented in Figure 6. The translational part of the rigid-body motion is not directly visible in the derivatives, but the difference in translation between rigid bodies contributes to the derivative fields in their interface regions.

The characterization of the elastic properties of proteins by decomposition of the normal modes has been studied previously.[38,39] Vector analysis of normal modes has also been used to analyze protein domains.[40] In that work, the displacement field was not evaluated on a regular grid and the curl was calculated per residue from the atomic displacements of four atoms; the other derivative fields were not used at all. Our method has several advantages as the definition of the vector fields on a regular grid by averaging eliminates high-frequency noise and provides a valuable visualization aid and the calculation of the strain and divergence fields helps in locating regions of high flexibility.

RESULTS AND DISCUSSION

Interresidue Distances

The asymmetric unit of ATCase is composed of the four chains C1, R1, C6, and R6. Despite this, the variations in the total interresidue distances due to the modes and those deduced from the comparison of crystal structures show the same trends in C1 and C6 and in R1 and R6 in both the T and R states. Consequently, only the total interresidue

distance variations in the C1 and R1 chains will be described and illustrated.

Figure 2 shows the total distance variations obtained from the low-frequency modes and from the comparison of the crystal R and T state structures. A general observation resulting from this figure is that the intradomain distances do not exhibit significant variations compared to the interdomain distances.

In the regulatory chain, the ZN and ALLO domains are structurally well defined and connected together by the flexible loop 98:101, which follows the S5′ strand and is backbone to backbone hydrogen bonded to strand S7′. The division of the regulatory chains into two domains is very clear from the analysis of the interresidue distance variations resulting from the NM study in Figure 2a. The ALLO and ZN domain boundaries, originally deduced from the sequence and from the position of the residues relative to the ligand binding sites, are confirmed by the NM analysis. Each domain in the regulatory chain exhibits almost no intraresidue distance variations and moves as a rigid unit relative to the other domain. These results confirm the previous analyses of the very low-frequency normal modes,[1,2] which show that the atoms of each domain move *en bloc* in some of the modes. Similar rigid-body behavior was observed for the ALLO domain from MD simulations.[17] The delineation of a protein into domains is not always straightforward and several methods have been developed for the task.[41–44] Recently, theoretical techniques (MD and cross-correlation matrix analyses) have allowed the identification of three domains in the cytochrome P450BM-3, whereas only two were determined from the crystal structure investigation.[44]

Surprisingly, the largest intradomain distance variations in Figure 2a are those involving the atoms of helix H2′ of the ALLO domain. The quaternary motions present at these frequencies are thus strongly coupled to the H2′ helix motion. This segment, lying close to the interdomain interface, makes hydrophobic interactions with segments S6′ and H3′ of the ZN domain. Site-directed mutagenesis studies have shown the crucial involvement of the H2′ helix in the ATP signal transmission.[45–47]; in particular, the mutation Y77 → F, located in the C-terminal end of helix H2′, produces an enzyme that is inhibited by ATP but reacts normally to CTP.[45] The special biological importance of this helix might be related to the particularly large motions that are present in the low-frequency modes.

In the catalytic chains, there is no clear dynamical delineation between domains; the distances that show large variations are not exclusively interdomain ones. This might be due to the fact that the CP and ASP domains are closely packed, connected by two stacked α-helices, H5 and H12, which cross each other by about 30°. A cluster of surrounding helices maintains this interface; helix H12, which is the largest one in ATCase and contains 20 residues, is blocked between the H2 and H1 helices, with crossing angles of about 15° and 30°, respectively. Helix H5 is maintained by the H6 and H1 helices and lies on the H11 helix. This particular configuration at the CP:ASP interface, rather typical of interfaces allowing shear motions,[48] limits the mobility of one domain relative to the other, as can be seen in Figure 2c. However, there are large changes in the interresidue distances which include atoms of the 80s and 240s loops, reflecting the large motions (of 5 and 10 Å, respectively) that these loops exhibit during the T → R transition. The motion of the region c[80–100] is strongly coupled to the quaternary motions arising at low frequencies. This segment, involved in the C1:C2 interface, is more flexible in the R state than in the T state; its motion is more coupled to the quaternary change in the R state than in the T state.

The flexibility of the phosphate binding region 50–55 that moves by about 2 Å upon PALA binding[4] is observed in the theoretical calculations and is more visible in the R state than in the T state. This region lies directly at the CP:ASP interface with the distances between the Cα of residues 53 and 54 and between phosphonoacetamide being less than 5 Å.[6] The mutations T55 → A, R54 → A, and S52 → A lead to enzymes with significantly reduced catalytic activity and affinity for aspartate and underline the crucial role of this region.[49] Furthermore, the bridging salt-link interactions between E50 and both R234 and R167 have been shown to be essential by site-specific mutagenesis studies[12,50] and a small angle X-ray scattering study.[51] A disruption of these interactions produces mutants with kinetic properties close to the T state enzyme: loss of cooperativity, decrease of activity, and reduced affinity for aspartate. These interdomain interactions were suggested to be essential for orienting the aspartate domain for aspartate binding and for positioning both substrates for catalysis.

The difference distance map between the T and R crystal structures (Fig. 2d) shows a close similarity to those obtained from the NM calculations, suggesting that the low-frequency modes are able to reproduce a significant part of the interdomain motions arising in the overall cooperative transition. In addition to the interdomain motions, the large motions of the 80s and 240s loops and the segment [50–55] are visible from a comparison of the T and R state crystal structures. Their motions are thus coupled to the overall structural change of the transition. In contrast, the intradomain motions of the helix H2′ in the regulatory chains do not appear in the comparison of the crystal structures, which suggests that while a displacement of these loops relative to the other atoms of the ALLO domain occurs at the beginning of the transition, the internal structure of the ALLO domain is restored once the other state is reached.

Backbone Dihedral Angle Variations

An indication of the internal flexibility of the domains may be obtained by examining the variations in the

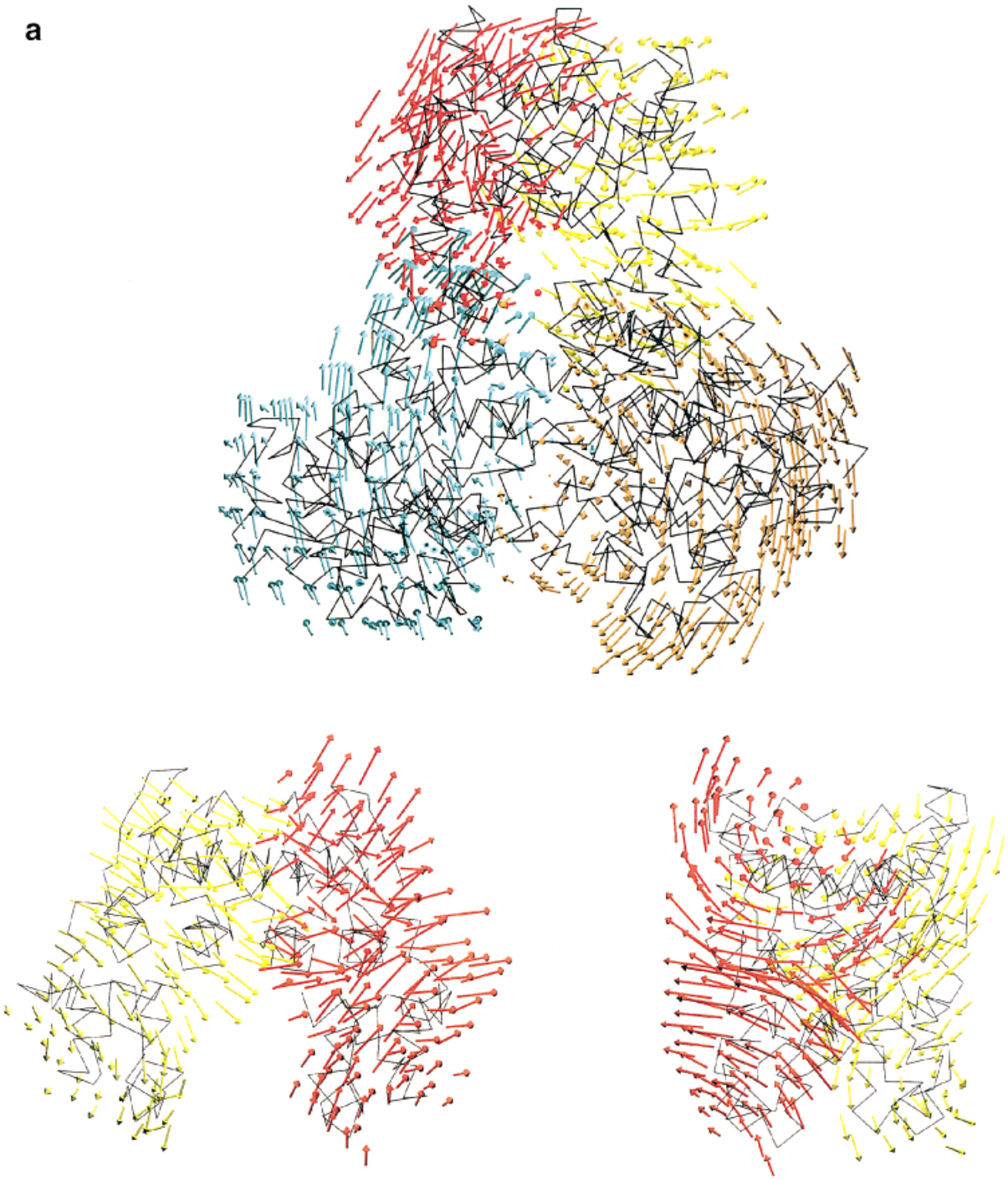

Fig. 5. **a: Upper figure:** the displacement field $\vec{u}$ in mode T_{15} for a selection of four chains—R1, red; R6, yellow; C1, blue; C4, brown. **Lower figures:** the displacement field $\vec{u}$ in mode R_{20} for a regulatory dimer, in two orientations differing by 90°. **b:** The curl $\vec{\nabla} \times \vec{u}$ of the vector field in mode T_9 for the R1 chain. **c:** The curl $\vec{\nabla} \times \vec{u}$ of the vector field in mode T_{15} for the C1 chain. In each figure, the vector fields are superimposed on a Cα trace of the appropriate structural element.

backbone dihedral angles resulting from either the low-frequency normal modes or the allosteric transition. The total dihedral angle changes due to the 47 modes are very similar among equivalent chains (data not shown) and so only the backbone deformations for the chains of the asymmetric unit are presented in Figure 3.

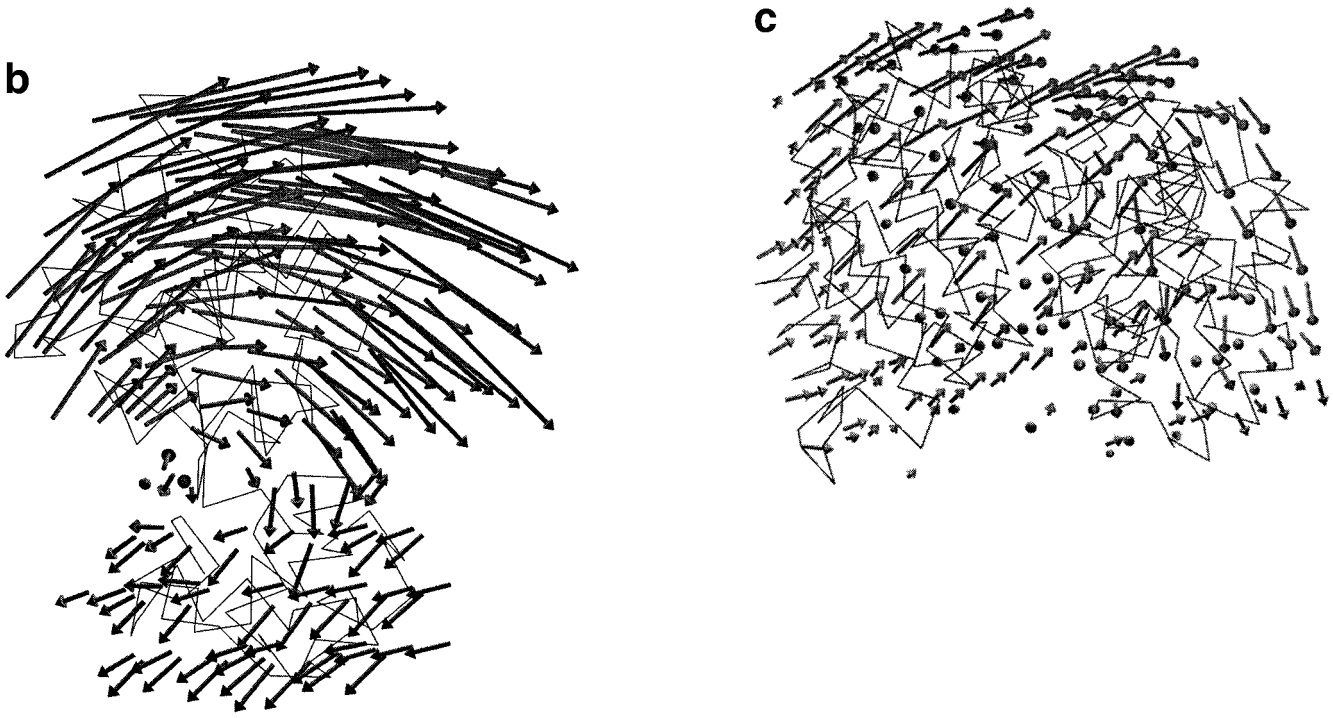

Figure 5. (Continued.)

In the regulatory chains, the comparison between the T and R state crystal structures shows that chains R1 and R6 have rather different dihedral angle changes although they both exhibit large backbone deformations in their C-terminal regions. It is these regions that are involved in the C1:R4 interface with the 240s loop of the catalytic chains and in the ZN:ALLO hydrophobic interface. In the T → R transition, the C1:R4 interface disappears, while the cleft at the ZN:ALLO interface enlarges. The ZN and ALLO domains are in contact through a hydrophobic interface in which rY77 is inserted into a pocket containing rL76, rV106, rL107, and rL151. In the R state, the interdomain hydrogen bonds between r153 and rK28 and between rY77 and rV106 disappear. Meanwhile, the H1′ helix [25–33] shifts along its axis by about 2.5 Å, giving a different interdigitation of the segment [31–33] relative to the segment [105–107].[4] These observations and the deductions from mutational effects at rL76 and rL151 have led to the proposal of a discriminating role of the ZN:ALLO interface in the effector signal transmissions even though it is located 12 Å away from the regulatory site.[45–47]

Reflecting these biochemical results, the backbone dihedrals of some residues lying at the ZN:ALLO interface are significantly modified by the low-frequency normal modes. In particular, the backbones of residues rL76 and rY77 show significant deformations. Both in the NM plots and in the comparison of the crystal structures, there are large backbone perturbations at residues rV106 and rL107. The segment r[128–132], which acts like a flap close to the H2′ helix in the T state, also shows some backbone deformations when the T and R crystal structures are compared. The backbones at segment r[96–97] located in the large loop connecting both domains and against the H2′ helix are also strongly deformed in the R modes of both the R1 and R6 chains.

Other backbone deformations can be related to their proximity to the allosteric binding site. These include the N terminus and the region r[50–53], which is part of the 50s loop. The deformation around the regulatory N terminus is only present in the comparison of the two crystal allosteric structures, while the deformation at r[50–53] is visible both in the T state modes of the R6 chain and in the comparison of the crystal structures of the two states.

The C1:R1 interface also exhibits some backbone flexibility as the backbone dihedrals in the r[128–132] region show large differences between the T and R state crystal structures. Indeed, the hydrogen bond rR128–cE204 is disrupted in the T state, while the hydrogen bond rR130–cD200 is rearranged into the hydrogen bond rR130–cE204.[4] The T state low-frequency modes deform the backbone at residue r128, but especially at residue rY140; this residue is hydrogen bonded to the residue cE117 in the R state only. Residue r118, also located at the C1:R1 interface, is also strongly deformed by the normal modes.

The low-frequency normal modes of the T state also affect the C1:R4 interface by deforming the backbones of residues r110 and r143 of chain R6. Residue rK143 interacts with residues cD236 and cS238. Its mutation into

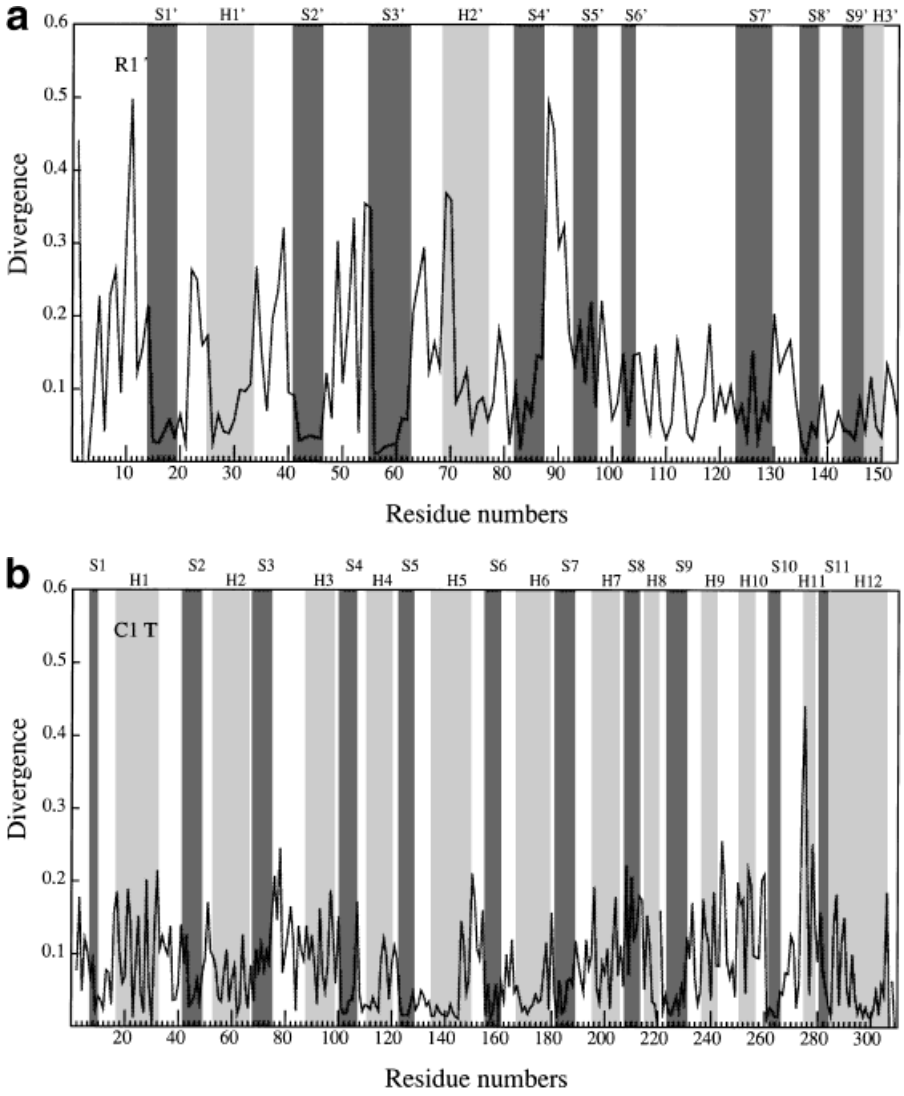

Fig. 6. Distribution of the total divergence on the residues. **a:** Due to the T modes on R1. **b:** Due to the T modes on C1. **c:** Due to the R modes on R1. **d:** Due to the R modes on C1.

alanine shifts the enzyme into an R-like conformation,[15] showing its importance in the stabilization of the T state.

In the catalytic chains, the crystal structure comparison shows that the backbone deformations in C1 and in C6 are located uniquely in the 80s and 240s loops, which are involved in the C1:C2 and C1:R4 interfaces, respectively. All the calculated modes in each allosteric state affect the backbone of the 80s loop, but the 240s loop is only deformed in the C1 chain and predominantly by the T state modes. The C1:C2 interface is deformed by the low-frequency modes, as shown by peaks in the segment c[268–270]. Small backbone deformations due to the modes can be seen at the CP:ASP interface at residues cR234 and cE50, which are hydrogen bonded in the R state only. The normal modes also change the backbone at residue c300, located in the interdomain bridging H12 helix.

The backbone deformations present at residues rY77, rV106, cE50, r[128–132], at the 80s loop, and seen from the NM simulations are in good correspondence with the backbone differences between the R and T state crystal structures. The other peaks resulting from backbone modifications due to the modes are not correlated with backbone differences between the R and T state crystal structures.

The incomplete correspondence between theoretical and experimental backbone perturbations is not surprising. The comparison of both crystal structures gives data about the overall structural changes caused by the transition,

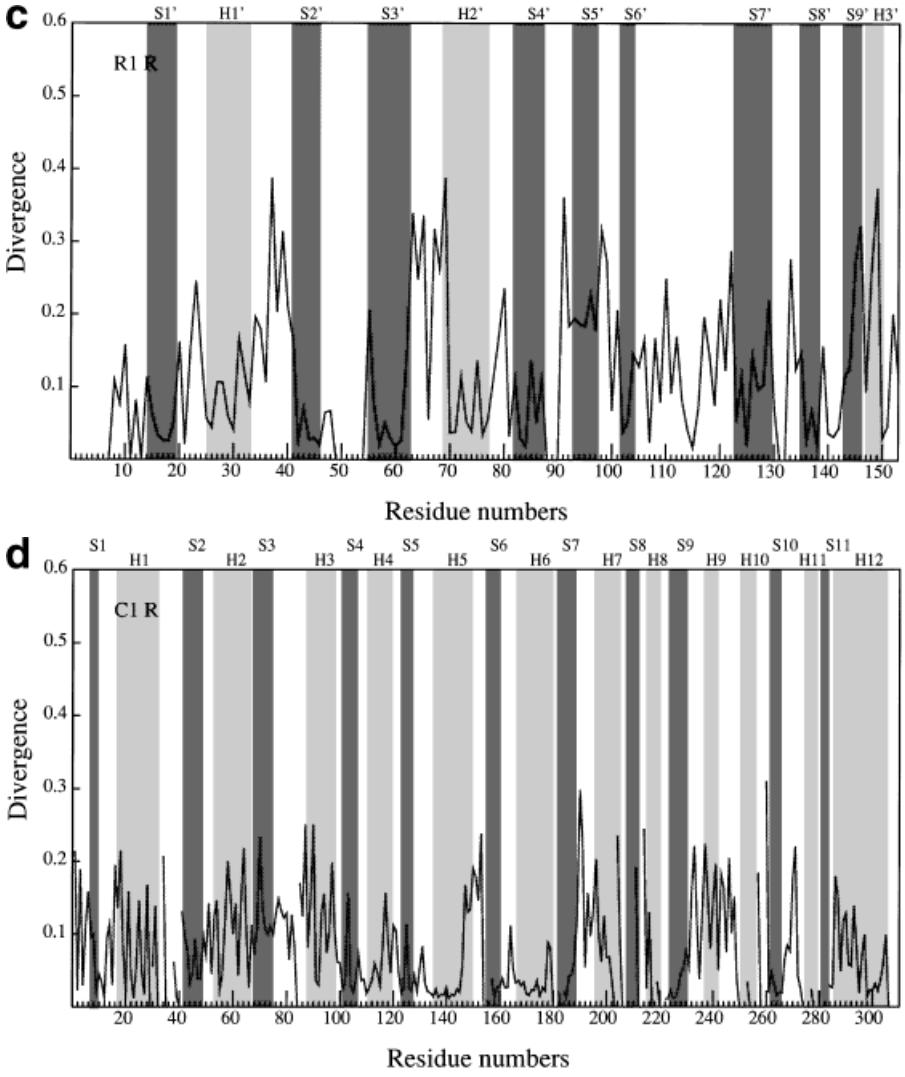

Figure 6. (Continued.)

while the NM analyses provide insights into the structural deformations that the two states can undergo which lead to the transition and so some of the local deformations that may be necessary in the early stages of the transition could be restored before the other state is reached. Furthermore, even though the calculated modes are able to reproduce to a large extent the large quaternary events occurring in the transition, they can only reduce the total RMS deviation between both states by about 4%.

In summary, we can say that the large-amplitude motions present at these frequencies are coupled to local motions involving specific residues, which may be key residues in the propagation of the delocalized motion. The higher frequency modes, which we neglect, give an additional local motion that will become rapidly decoupled from the global motion as the frequency increases. This implies that we are likely to be overestimating the coupling between the "total" local and global motions.

Interdomain Rotations

The differences in interdomain rotation angles are presented in Table II. How they were calculated is described in Materials and Methods. The minimization procedures were designed to produce deviations as small as possible from the crystal structures (by 3.15 and 2.42 Å on the backbone atoms in the R and T state structures, respectively[1,2]) and to maintain the C_3 symmetry. Even so, the minimized structures do show some perturbations in the quaternary structure, especially in the relative arrangement of domains in the regulatory chains. It must be noted

that a drastic minimization process leading to an energy gradient close to 10^{-5} kcal/mol. Å was a necessary requirement of the NM calculations.

The effect of the modes on the difference in interdomain rotation angles is presented in Figure 4. In both states, the rotation angles between the ALLO and ZN domains are perturbed to a larger extent than the angle between the ASP and CP domains, which show more constant and smaller changes. The differences shown in the interdomain rotations are consistent with the flexibilities of the domain interfaces discussed above. In both states, the 15 lowest frequency modes have the greatest effect on the cleft opening/closure of the regulatory chains. The modes perturb by at most 1° the interdomain rotation in the regulatory chains and by 0.4° the equivalent angle in the catalytic chains.

Vector-Field Analysis of Structural Deformations

The technique of vector-field analysis, described in Materials and Methods, allows a graphical representation of the structural deformations and rigid-body movements occurring in the modes. Figure 5 illustrates a selection of the local deformations and rotations due to some of the modes that previously were found to be important in generating the transition.[1,2]

The local displacement field in mode T_{15} illustrated in Figure 5a shows that there is an opposite local rotation in C1 and C4, and that the motion propagates through the C1:C4 interface, even though its amplitude is less in the interface area. This mode combines a screw motion of the regulatory chains, a contrarotatory motion of the catalytic subunits, and a movement that reduces the distance between the catalytic chains. Together these generate a gear-wheel motion that is very close to the description of the mechanism of the quaternary transition made by Perutz[23] from observations of the crystal structures. This mode and its analog in the R state, R_{17}, contribute most to the transition.[1,2] The local rotation field indicates that the ALLO dimers rotate around an axis parallel to the pseudo-C_2 axis, while the ZN domains have less important local rotations around another axis.

The displacement field generated by the R_{20} mode for a regulatory dimer is shown in Figure 5a. The diffusion of the motion through the R1:R6 interface is clear as well as the change in the direction of the motion which occurs around the ZN:ALLO interface. In this mode, the catalytic chains undergo a breathing motion at the C1:C4 and C1:R1 interfaces which is coupled to the opening motion within the regulatory chains.

The coupling between the quaternary rearrangements and tertiary motions is clear from Figure 5b and Figure 5c, which show the rotation fields in mode T_9 for the R1 chain and in mode T_{15} for the C1 chain, respectively. The characteristics of mode T_9 are a rigid-body motion of the whole allosteric 10-stranded sheet, large fluctuations in the 240s loop, an important modification of the C1:R4 interaction energy, and the strongest displacement of the T structure toward the R structure in terms of RMS difference.[1,2] The displacement field of this mode exhibits a large deformation of the allosteric dimers and only weak motion in the rest of the protein. The local rotation field indicates a clear delimitation at the ALLO:ZN interface. The rotations within each domain of the regulatory chain are homogeneous but they are in opposite directions relative to one another. The curl of the C1 chain due to the T_{15} mode shows that, like the displacement field of Figure 5a, the quaternary motions produced by this mode are coupled to a relative motion of the ASP and CP domains.

The total divergence due to all modes in each state is presented in Figure 6. We only present the distribution of this quantity on residues of the R1 and C1 chains, as the total divergence is similar among the catalytic chains and among the regulatory chains.

The modes affect the local density in the T and R state structures in a similar way. The divergence is generally lower in the structured secondary elements than in the neighboring loops, especially in the regulatory chains. The fluctuations are strong and vary a lot between neighboring residues. The elements showing the highest divergence are S5′ and H3′ in the regulatory chains and H11 and H7 in the catalytic chains. The low-frequency motions are thus coupled to preferential density changes in these elements. It is interesting to note that in the H5 and H12 helices, which "cross and link" the ASP and CP domains, the divergence exhibits a two-plateau behavior. The beginning of H5 and the end of H12, both closer to the CP domain, show little divergence, in contrast to their parts closer to the ASP domain. Overall, the differences in density changes are not very significant. In general, our experience shows that this is a usual feature of the density changes that occur in protein motions due to displacement fields averaged over the atoms in cubes of 5 Å a side. It is possible to analyze density fluctuations on a finer scale, but this requires other techniques that we are currently developing in the laboratory.

CONCLUSION

This article identifies the quaternary and tertiary structural changes resulting from the low-frequency mode motions of the R state ATCase ligated to CTP, phosphoacetamide, and malonate, and of the CTP-ligated T state ATCase. The normal modes of these systems have been calculated previously.[1,2] At the lowest frequencies (0.5 cm^{-1}), corresponding to a time scale of 70 ps, ATCase clearly exhibits rigid-body motions. Studying such low-frequency motions by molecular dynamics would require very long simulation runs to attain sufficient sampling. NM analysis is thus very appropriate in this context. A detailed quantitative analysis of the mode motions showed their ability to promote the changes that occur during the transition at a quaternary level.

This work is a complement to our two earlier studies in which we highlighted large scale quaternary motions. Here we investigate the impact of the lowest frequency mode motions on smaller scale structures using analyses of the variations in interresidue distances, of deformations of the backbone dihedral angles, and of the atomic displacements. We concentrate on the form of the large amplitude motions rather than on their associated frequencies since effects, such as solvent damping, would likely modify these.

There are strong interdomain motions in both the catalytic and regulatory chains in the frequency range studied which agree rather well with the crystallographic data. The domain boundaries for the regulatory chains obtained from the NM study are in good agreement with those normally proposed. In the catalytic chain, the domain boundaries between the CP and ASP domains are less clear. This is probably due to their dense packing and their interconnection by two crossed α-helices and means that the total domain closure results from numerous and more localized motions. The NM results show that the interdomain motions of the catalytic and regulatory chains are coupled so that the control of the regulatory chain will affect the interdomain motion of the catalytic domains and therefore the catalytic efficiency.

The normal modes reveal that some specific segments show a strong dynamical coupling with the quaternary changes present at frequencies below 5 cm^{-1}: in particular, the 80s and 240s loops, the segment [50–55], and the helix H2′. This dynamical coupling finds a functional echo via mutagenesis and crystallographic studies. The segment [50–55], located at the CP:ASP interface, has been shown to be critical for the catalytic activity and affinity for aspartate.[50] It moves by about 2 Å upon PALA binding.[4] The helix H2′, lying at the ZN:ALLO interface, is critical in the transmission of the heterotropic signal.[45–47]

The low-frequency modes substantially alter the backbone dihedrals of some residues. These residues are located mainly, but not exclusively, at the interfaces. The overall global motions in ATCase at frequencies below 5 cm^{-1} are coupled with more localized motions involving specific residues, which are mainly at the ZN:ALLO, C1:R1, C1:C2, and C1:R4 interfaces. Some residues have their backbone modified in both the normal modes and in the overall crystal transition: this is the case for the residues rV106 and rL107, which are located at the ZN:ALLO interface.

On a more general level, one of the major aims of work on the allosteric transition in ATCase is the identification of the signal transmission pathway. The nature of these pathways is unknown but mutagenesis studies indicate that communication between different parts of the protein has a certain plasticity. The double mutant cE50A–cS171A, in which CP:ASP bridging interactions are disrupted, shows some enhancement of homotropic cooperativity with respect to aspartate relative to the single mutant enzymes.[52] The double mutant cE239Q–rY77F, which combines R state and T state shifter mutations, has wild-type specific activity, one mutation compensating the other, which supports the notion that direct pathways for transmission of the heterotropic signals are unlikely.[53] Such plasticity has also been hypothesized from an analysis of the electronic network of interactions which provides multiple and alternative potential mechanisms for transmitting to remote sites the perturbation due to the allosteric signal or to a single mutation.[54]

If it is assumed that the signal is due to structural deformations in the molecule, it is clear from the analysis of the NM motions and from the visualization of their displacement and rotation fields that our calculations support the concept of diffuse and multiple pathways through which information is transmitted from one part of a molecule to another. However, some specific residues show particular structural flexibility during the low-frequency modes. The coupling between these local motions and the overall delocalized motion is unexpected. It suggests that the residues showing higher flexibility may be centers of the overall motion and the total cooperative transition may itself be decomposed into a large-amplitude phenomena relayed more specifically by these key residues. This hypothesis has the advantage of reconciling both the effects of compensative double mutations and the preferential regulatory signal path.

ACKNOWLEDGMENTS

We thank Guy Hervé and Raymond Cunin for fruitful discussions and the Institut de Biologie Structurale—Jean-Pierre Ebel (CNRS/CEA) and the Human Frontiers Science Program (K.H.) for support. A grant of computer time from the IDRIS Center (Institut du Développement et des Ressources en Informatique Scientifique) made possible the normal mode calculations. We also acknowledge the referees for helpful comments.

REFERENCES

1. Thomas A, Field MJ, Mouawad L, Perahia D. Analysis of the low-frequency modes of the T-state of aspartate transcarbamylase. J Mol Biol 1996;257:1070–1087.
2. Thomas A, Field MJ, Perahia D. Analysis of the low-frequency modes of the R state of aspartate transcarbamylase and a comparison with the T state modes. J Mol Biol 1996;261:490–506.
3. Lipscomb WN. Activity and regulation in aspartate transcarbamylases. Proc. Robert A. Welch Found. Conf Chem Res 1992;36:103–143.
4. Lipscomb WN. Aspartate transcarbamylase from *Escherichia coli:* Activity and regulation. Adv Enzymol Relat Areas Mol Biol (U.S.A.) 1994;68:67–151.
5. Schachman HK. Aspartate transcarbamoylase. Curr Opin Struct Biol 1993;3:960–967.
6. Kim KH, Pan Z, Honzatko RB, Ke H-M, Lipscomb WN. Structural asymmetry in the CTP-liganded form of aspartate carbamoyltransferase from *Escherichia coli.* J Mol Biol 1987;196:853–875.
7. Gouaux JE, Stevens RC, Lipscomb WN. Crystal structures of aspartate carbamoyltransferase ligated with phosphonoacetamide, malonate, and CTP or ATP at 2.8 Å resolution and neutral pH. Biochemistry 1990;29:7702–7715.

8. Fetler L, Vachette P, Hervé G, Ladjimi MM. Unlike quaternary structure transition, the tertiary structure change of the 240s loop in allosteric aspartate transcarbamoylase requires active site saturation by substrate for completion. Biochemistry 1995;34: 15654–15660.
9. Collins KD, Stark GR. Aspartate transcarbamylase. Studies of the catalytic subunit by ultraviolet difference. J Biol Chem 1969;244: 1869–1877.
10. Griffin JH, Rosenbusch JP, Weber KK, Blout ER. Conformational changes in aspartate transcarbamylase. I. Studies of ligand binding and of subunit interactions by circular dichroim spectroscopy. J Biol Chem 1972;247:6482–6490.
11. Stevens RC, Lipscomb WN. A molecular mechanism for pyrimidine and purine control of aspartate transcarbamylase. Proc Natl Acad Sci USA 1992;89:5281–5285.
12. Stevens RC, Chook YM, Cho CY, Lipscomb WN, Kantrowitz ER. *Escherichia coli* aspartate carbamoyltransferase: The probing of crystal structure analysis via site-specific mutagenesis. Protein Eng 1991;4:391–408.
13. Lee BH, Ley BW, Kantrowitz ER, O'Leary MH, Wedler FC. Domain closure in the catalytic chains of *Escherichia coli* aspartate transcarbamoylase influences the kinetic mechanism. J Biol Chem 1995;270:15620–15627.
14. Newton CJ, Kantrowitz E. Importance of domain closure for homotropic cooperativity in *Escherichia coli* aspartate transcarbamylase. Biochemistry 1990;29:1444–1451.
15. Eisenstein E, Markby DW, Schachman HK. Heterotropic effectors promote a global conformational change in aspartate transcarbamoylase. Biochemistry 1990;29:3724–3731.
16. Svergun DI, Barberato C, Koch MHJ, Fetler L, Vachette P. Large differences are observed between the crystal and solution quaternary structures of allosteric aspartate transcarbamylase in the R state. Proteins 1997;27:110–117.
17. Tanner JJ, Smith PE, Krause KL. Molecular dynamics simulations and rigid body (TLS) analysis of aspartate carbamoyltransferase: Evidence for an uncoupled R state. Protein Sci 1993;2:927–935.
18. Case DA. Normal mode analysis of protein dynamics. Curr Opin Struct Biol 1994;4:285–290.
19. Gibrat J-F, Gô N. Normal mode analysis of human lysozyme: Study of the relative motion of the two domains and characterization of the harmonic motion. Proteins 1990;8:258–279.
20. Mouawad L, Perahia D. Motions in hemoglobin studied by normal mode analysis and energy minimization: Evidence for the existence of tertiary T-like, quaternary R-like intermediate structures. J Mol Biol 1996;258:393–410.
21. Faure P, Micu A, Perahia D, Doucet J, Smith JC, Benoit JP. Correlated intramolecular motions and diffuse X-ray scattering in lysozyme. Struct Biol 1994;1:124–128.
22. Lamy AV, Souaille M, Smith JC. Simulation evidence for experimentally detectable low-temperature vibrational inhomogeneity in a globular protein. Biopolymers 1996;39:471–478.
23. Perutz MF. Mechanisms of cooperativity and allosteric regulation in proteins. Q Rev Biophys 1989;22:139–236.
24. Kosman RP, Gouaux JE, Lipscomb WN. Crystal structure of CTP-ligated T state aspartate transcarbamylase at 2.5 Å resolution: Implications for ATCase mutants and the mechanism of negative cooperativity. Proteins 1993;15:147–176.
25. Brünger AT, Karplus M. Polar hydrogen positions in proteins: Empirical energy placement and neutron diffraction comparison. Proteins 1998;4:148–156.
26. Zanotti G, Monaco HL, Foote J. Structure of the inhibitor of aspartate transcarbamylase N-(phosphonoacetyl)-L aspartate. J Am Chem Soc 1984;106:7900–7904.
27. Brooks BR, Bruccoleri RE, Olafson BD, States DJ, Swaminathan S, Karplus M. CHARMM: A program for macromolecular energy, minimization and dynamics calculations. J Comp Chem 1983;4: 187–217.
28. Loncharich RJ, Brooks BR. The effects of truncating long-range forces on protein dynamics. Proteins 1989;6:32–45.
29. Steinbach PJ, Brooks BR. New spherical-cutoff methods for long-range forces in macromolecular simulation. J Comp Chem 1994;15:667–683.
30. Mouawad L, Perahia D. Motions in hemoglobin studied by normal mode analysis and energy minimizations. Evidence for the existence of tertiary T-like, quaternary R-like intermediate structures. J Mol Biol 1996;258:393–410.
31. Mouawad L, Perahia D. Diagonalization in a mixed basis: A method to compute low-frequency normal modes for lage macromolecules. Biopolymers 1993;33:599–611.
32. Perahia D, Mouawad L. Computation of low-frequency normal modes in macromolecules: Improvements to the method of diagonalization in a mixed basis set. Application to hemoglobin. Comput Chem 1995;19:241–246.
33. Guilbert C, Pecorari F, Perahia D, Mouawad L. Low frequency motions in phosphoglycerate kinase. A normal mode analysis. Chem Phys 1996;204:327–336.
34. Wilson EB, Jr, Decius JC, Cross PC. "Molecular Vibrations." New York: Dover Publications, 1955.
35. Kabsch W. A solution for the best rotation to relate two sets of vectors. Acta Crystallogr 1976;A32:922–923.
36. Kabsch W. A discussion of the solution for the best rotation to relate two sets of vectors. Acta Crystallogr 1978;A34:827–828.
37. Hinsen K. The molecular modeling toolkit: A case study of a large scientific application in Python. Proceedings of the 6th International Python Conference, 1997.
38. Gô N, Noguti T, Nishikawa T. Dynamics of a small globular protein in terms of low-frequency vibrational modes. Proc Natl Acad Sci USA 1983;80:3696–3700.
39. ben-Avraham D, Tirion MM. Dynamic and elastic properties of F-actin: A normal modes analysis. Biophys J 1995;68:1231–1245.
40. Hayward S, Kitao A, Berendsen HJC. Model-free methods of analyzing domain motions in proteins from simulation: A comparison of normal mode analysis and molecular dynamics simulation of lysozyme. Proteins 1997;27:425–437.
41. Nichols WL, Rose G, Eyck LFT, Zimm BH. Rigid domains in protein: An algorithmic approach to their identification. Proteins 1995;23:38–48.
42. Islam SA, Luo J, Sternberg MJ. Identification and analysis of domains in proteins. Protein Eng 1995;8:513–525.
43. Wriggers W, Schulten K. Protein domain movements: Detection of rigid domains and visualization of hinges in comparisons of atomic coordinates. Proteins 1997;29:1–14.
44. Arnold GE, Ornstein RL. Molecular dynamics study of time-correlated protein domain motions and molecular flexibility: Cytochrome P450BM-3. Biophys J 1997;73:1147–1159.
45. Van Vliet F, Xi XG, Ladjimi MM, et al. The heterotropic interactions in aspartate transcarbamylase turning allosteric ATP activation into inhibition as a consequence of a single tyrosine to phenylalanine mutation. Proc Natl Acad Sci USA 1991;88:9180–9183.
46. Xi XG, Van Vliet F, Ladjimi MM, et al. Heterotropic interactions in *Escherichia coli* aspartate transcarbamylase. Subunit interfaces involved in CTP inhibition and ATP activation. J Mol Biol 1991;220:789–799.
47. Xi XG, De Staerke C, Van Vliet F, et al. The activation of *Escherichia coli* aspartate transcarbamylase by ATP. Specific involvement of helix H2′ at the hydrophobic interface between the two domains of the regulatory chains. J Mol Biol 1994;242:139–149.
48. Gerstein M, Lesk AM, Chothia C. Structural mechanisms for domain movements in proteins. J Mol Biol 1994;33:6739–6749.
49. Stebbins JW, Robertson DE, Roberts MF, Stevens RC, Lipscomb WN, Kantrowitz ER. Arginine 54 in the active site of *Escherichia coli* aspartate transcarbamoylase is critical for catalysis: A site-specific mutagenesis, NMR, and X-ray crystallographic study. Protein Sci 1992;1:1435–1446.
50. Ladjimi MM, Middleton SA, Kellher KS, Kantrowitz ER. Relationship between domain closure and binding, catalysis and regulation in *E. coli* aspartate transcarbamylase. Biochemistry 1988;27: 268–276.

51. Tauc P, Keiser RT, Kantrowitz ER, Vachette P. Glu-50 in the catalytic chain of *Escherichia coli* aspartate transcarbamoylase plays a crucial role in the stability of the R quaternary structure. Protein Sci 1994;3:1998–2004.
52. Baker DP, Fetler L, Vachette P, Kantrowitz ER. The allosteric activator ATP induces a substrate-dependent alteration of the quaternary structure of a mutant aspartate transcabamoylase impaired in active site closure. Protein Sci 1996;5:2276–2286.
53. Aucoin JM, Pishko EJ, Baker DP, Kantrowitz ER. Engineered complementation in *Escherichia coli* aspartate transcarbamoylase. J Biol Chem 1996;47:29865–29868.
54. Oberoi H, Trikha J, Yuan X, Allewell NM. Identification and analysis of long-range electrostatic effects in proteins by computer modeling: Aspartate transcarbamylase. Proteins 1996;25:300–314.
55. Ke HM, Lipscomb WN, Cho Y, Honzatko RB. Complex of N-phosphonoacetyl-1-aspartate with aspartate transcarbamylase. X-ray refinement, analysis of conformational changes and catalytic and allosteric mechanisms. J Mol Biol 1988;204:725–747.
56. Kraulis PJ. MOLSCRIPT: a program to produce both detailed and schematic plots of protein structures. J Appl Crystallog 1991;24: 946–950.